A major purpose of the Technical Information Center is to provide the broadest dissemination possible of information contained in DOE's Research and Development Reports to business, industry, the academic community, and federal, state and local governments.

Although a small portion of this report is not reproducible, it is being made available to expedite the availability of information on the research discussed herein.

LA-UR--85-2454

DE85 015714

CONF-8509129--2

TITLE EXPERIMENTS WITH NON-DARCY FLOW IN JOINTS WITH LARGE SCALE ROUGHNESS

AUTHOR(S) David K. Cornwell and Hugh D. Murphy

SUBMITTED TO International Symposium on Fundamentals of Rock Joints, Bjorkliden, Lapland, Sweden, September 15-20, 1985.

Los Alamos National Laboratory
Los Alamos, New Mexico 87545

EXPERIMENTS WITH NON-DARCY FLOW IN JOINTS WITH LARGE SCALE ROUGHNESS

David K. Cornwell and Hugh D. Murphy
University of California
Los Alamos National Laboratory
Los Alamos, New Mexico 87545

ABSTRACT

Understanding the fluid flow characteristics of joints is important in connection with any process requiring flow through geological media. Examples include geothermal energy reservoirs and underground waste repositories. Joints are normally in contact at roughness asperities; consequently the relative roughness, the ratio of the asperity protrusion to the mean flow aperture, is approximately one, which is orders of magnitude greater than that encountered in more usual situations such as pipe and channel flows. In our experiments the joint roughness was idealized with sawtooth corrugations. The mean flow aperture could be independently varied, allowing study of relative roughness effects, and the phase lag of the opposing corrugation peaks could also be varied, so that experiments could be carried out with peak-to-peak alignment, peak-to-valley alignment, or any combination thereof.

We found that Darcy's Law became invalid for Reynolds numbers greater than about 100. Hence, for most of our studies the flow was non-Darcian, and so we adopted the usual convention of representing pressure losses in terms of an apparent friction factor. When the roughness peaks were aligned, resulting in maximum flow disturbance, the friction factor increased when the relative roughness was increased, simulating the closure of a joint due to normal-direction loading. However, when the roughness peaks were 180° out of phase, so that peaks were opposite valleys, the friction factor initially increased with greater relative roughness, but then decreased -- this apparent paradox is explained as follows. When the relative roughness is small, the velocity vectors for much of the flow are parallel to the mean flow direction. The sawtooth peaks then represent a local disturbance to the mean flow, and as expected, increased roughness represents increased eddying and pressure loss. However, as relative roughness is increased, eventually the flow streamlines are forced to become parallel to the alternating sawtooth surfaces so the flow is "channeled", resulting in a series of disjointed, but individually smooth micro-channels with 90° turns between each micro-channel. Intermediate phase angles i.e., peaks not completely in or out of phase, yielded combinations of the effects observed in the peak-to-peak and peak-to-valley situations.

1.0 INTRODUCTION

Fractures and natural joints tend to close under the influence of tectonic compressive stresses. The residual opening is provided by the contact of roughness, e.g. rock grains, on the opposing fracture surfaces. Thus the projection of the roughness into the flow stream is of the same order as the fracture opening itself. The goal of this research was to examine the effect of such large scale roughness on the pressure loss-hydraulic flow rate charac-

teristics of fractures. A cursory look at fractures and natural joints in outcroppings indicates that surface roughness defies easy characterization. Not only do the roughness dimensions perpendicular and parallel to the flow stream vary widely, but the shape and distribution of the roughness also differ considerably. Geologically recent fractures often have sharply disjointed surfaces, and the individual roughnesses are angular and crag-like, whereas old fractures are weathered and worn, and usually have undergone geochemical reactions at the fracture surfaces, so that the roughnesses are smooth and round. This investigation was initially motivated by application to fractured geothermal energy reservoirs where the rock would be hydraulically fractured to create the required permeability. Typically this is done in geothermal reservoirs by drilling into low permeability basement rock to a depth hot enough to be useful and pressurizing the well above the compressive tectonic stresses of the surrounding rock. Consequently our interest was in the angular and crag-like roughnesses. Rather than attempt to match an actual fracture surface, which would not be representative of other surfaces to be encountered, we elected to simulate fractures with a uniformly periodic sawtooth surface. While this is admittedly a great simplification it offers three important advantages:

1. A regular sawtooth surface is easily fabricated and characterized; the results can be interpreted without regard to potential geometrical ambiguities; and, if need be, this surface can be reproduced and the experiments repeated elsewhere.

2. Theoretical predictions are available through computer codes which solve the exact Navier Stokes equation for the sawtooth configuration used in this study.

3. Even though it represents a simplification, flow over a sawtooth surface exhibits most of the features of flow over real fracture surfaces.

2.0 EXPERIMENTAL APPARTUS

Figure 1 is a photograph of the test section and Figure 2 is a drawing showing the flow surfaces in more detail. For compactness Figure 2 shows the test section in a horizontal configuration, whereas it was actually mounted vertically, as shown in Figure 1. A blower was used in its reverse (suction) mode to draw air from the room between the two sawtooth-roughened plates, then through the transition shown near the bottom of Figure 1, smoothly guiding the flow from the vertically mounted test section to the horizontal circular tube shown in the lower right hand corner. While not shown in the photo, this circular tube carries the air flow to a laminar flow measuring element, control valves, and eventually to the reversed blower where air is exhausted back to the room. While water is likely to be used in actual underground applications, in the present study air was experimentally more convenient. In all cases the pressure drop was less than 2 k Pa, so the air could be treated as an incompressible fluid, thus satisfying the major condition for experimental similitude.

One of the test section plates is aluminum and the other is plexiglas. The aluminum plate afforded easy fabrication while the transparent plexiglas allowed flow visualization. The plates are both 0.685 m long in the vertical, or streamwise direction and 0.152 m wide in the horizontal, or span, direction. The sawtooth corrugations are symmetrical right angle triangular prisms with a 6.35 mm base, a 3.18 mm height, and a width which stretches the entire 0.152 m span. The aluminum plate has 16 pressure taps arrayed in the flow direction which are 38 mm apart, corresponding to six complete

corrugations between taps. The first tap is 38.1 mm from the entry. At 76.2 mm and at 546.1 mm downstream of the inlet there are three taps; one is at the longitudinal center of the section and the other two are 50.8 mm from the side edges. These extra taps are used to check that pressure was invariant in the span direction. Pressures were measured with an MKS Baratron capacitance manometer with a resolution of 0.13 Pa.

Separating the aluminum and plexiglas plates are spacers at the edges which were used to control the distance between plates. The spacers can be seen in Figure 3, and several sizes were fabricated so as to result in spacings of 6.35, 5.08, 3.81, 3.18, 1.54, and 1.27 mm. As shown in Figure 3, neoprene O-ring seals were inserted between the spacers and the plates to prevent leaks. Before each experiment the apparatus was checked for leaks with a titanium tetrachloride smoke gun, and observed leaks were eliminated with sealing compound and vacuum grease.

The transition section shown near the bottom of Figure 1 is also made of plexiglas and directs the flow from the vertical test section and gradually reshapes the flow into a horizontal 76 mm diameter plexiglas tube which serves as the entry to the flow meter. The flow rate was determined by using one of three laminer flow elements (LFEs). These LFEs provided a flow rate range from 4×10^{-6} to 6×10^{-3} m^3/s which allowed the attainment of Reynolds numbers from 1 to 4000. Flow rates were further controlled by a throttle valve in the 76 mm (three-inch) diameter tube downstream of the flow meter.

In addition to the plate spacing, the other adjustable variable is the phase angle. As shown in Figure 4, the phase angle can be changed by displacing one of the plates relative to the other. In this manner runs were made when the peaks were aligned, $\phi = 0°$; when peaks and valleys were aligned, $\phi = 180°$; and at intermediate phase angles of 15, 30, 45, 60, 120, and 150°. Occasional checks at $\phi = 360°$, which presents the same geometry as $\phi = 0°$, indicated that overall precision of the experiment was better than 5%.

3.0 METHOD OF APPROACH

Following the usual treatment of flow in both smooth and rough ducts we present our measured pressure results in terms of friction factors, Reynolds numbers and relative roughness.

3.1 Friction Factor. The friction factor, f, is defined in terms of the pressure gradient, dp/dx, mean velocity V, and fluid density ρ.

$$f = \frac{2\, dp/dx}{t\rho V^2}$$

and V is defined as Q'/(2t), where Q' is the flow rate per unit span or width of the flow channel, and 2t is the average flow spacing between the two plates.

3.2 Reynolds Number. Following the usual convention the Reynolds number, Re, is defined in terms of the equivalent hydraulic diameter, D, defined as four times the average flow passage area divided by the perimeter. Consequently, $D = 4t$, and $Re = 4Vt/\nu$, where ν is kinematic viscosity.

3.3 Relative Roughness. The relative roughness, k/D is the projection of the roughness into the mean flow field divided by the equivalent hydraulic diameter. In all cases k was 3.18 mm, the height of the sawtooth corrugations.

4.0 RESULTS

4.1 Sawtooths Aligned peak-to-peak, $\phi = 0°$. The experimental data at $\phi = 0$ was limited by the physical constraint that when k/D = 0.51, the peaks were touching in line-to-line contact, creating a flow area approaching zero. Consequently an infinitely large

friction factor would be expected. Of the six spacings available in this study only three, with relative roughnesses of 0.26, 0.32, and 0.43, were large enough to avoid contact at $\phi = 0°$. The data are presented in Figure 5, and as expected, the friction factor increases as the relative roughness increases. The transition from the linear regime in which pressure loss scales with velocity or flow rate, ($f \sim Re^{-1}$), to the quadratic regime when pressure loss scales with square of velocity ($f \sim$ constant) occurs at a Reynolds number of approximately 50 for $k/D = 0.43$. The transitions for $k/D = 0.26$ and $k/D = 0.32$ lie between 300 and 700. These transitions are not necessarily laminar-to-turbulent flow transitions, but simply the Reynolds number range over which inertial effects due to accelerations and decelerations at the contractions and expansions began to dominate pressure losses, so that the flow becomes a "non-Darcy" one. The transition at a lower Reynolds number for the highest roughness case was caused by the greater flow disturbance. At $k/D = 0.43$, the ratio of the minimum area to the maximum area is 0.091, whereas the ratios of areas for $k/D = 0.32$ and 0.26 are 0.231 and 0.333, respectively. Pressure losses due to separation effects, wherein energy dissipation is enhanced, are much greater in the case when the peaks are nearly touching.

The predictions shown as solid lines in Figure 5 are based on the work of Lomize (1951) who found that the friction factor, using present nomenclature, was:

$$f = \frac{24}{Re}\left[1 + 17\,(k/D)^{1.5}\right].$$

In the absence of roughness, $f = 24/Re$ is the expected friction factor for laminar flow. The present data consistently lies above the Lomize relationship, probably because the sharp cornered, sawtooth roughness of the present study results in more flow disturbance than the rounder, sinusoidal roughness of Lomize's study.

4.2 Peaks and Valleys Aligned, $\phi = 180°$. Experiments at $\phi = 180°$ are of particular interest because when the spacing becomes small the flow can be viewed, as in Figure 6, as a series of micro-channels which are joined by right angle turns. The flow in an individual micro-channel is smooth, albeit interrupted at its ends by abrupt 90° turns. When the Reynolds number is small enough even the disturbances caused by these abrupt turns can be ignored, so that for all practical purposes the flow can be represented as smooth flow through an equivalent, stretched-out straight channel. As indicated on the right-hand side of Figure 6, the spacing in the smooth channel equivalent is $1/\sqrt{2}$ times that of the mean spacing, 2t, that was previously used. Furthermore, the smooth channel velocity will be $\sqrt{2}$ times the mean velocity, V, previously defined, and the stretched-out length of the equivalent channel equivalent will also be $\sqrt{2}$ times greater than the shorter apparent length of the actual situation. Now the friction factor of the smooth channel equivalent is 24/Re when using the appropriate velocity and spacing, but if we retain the previously defined nomenclature, it can be shown that while there is no change in the Reynolds number, the equivalent smooth tube friction factor is doubled, $f = 48/Re$.

Results for $\phi = 180°$ are summarized in Figure 7 and in Table 1. Note that as the relative roughness increases from 0.26 to 0.43 the friction factor linear flow increases but thereafter f actually decreases, indicating that the flow is beginning to behave as it would in a series of smooth micro-channels. At the highest relative roughness, $k/D = 1.26$, the friction factor was nearly equivalent to that expected in a perfectly smooth channel. Values of the transition Reynolds number show a similar effect. At low relative roughness linear flow

Table 1.
Summary of Runs at $\phi = 180°$; Peak-To-Valley Alignment

Relative Roughness	Linear Flow Friction Factor	Range Of Reynolds Number Over Transition From Linear To Quadratic Flow	Quadratic Flow Friction Factor
0.26	90/Re	250-700	0.4
0.32	150/Re	300-600	1.5
0.43	65/Re	30- 60	4.0
0.51	65/Re	30-100	2.6
0.64	70/Re	75-100	1.5
1.26	50/Re	250-300	0.5

is sustained to larger values of Re, in the range 250 to 750; at intermediate roughness the flow is more disturbed and transition occurs at Re as low as 30; but at very high roughness the stretched-out, smooth channel viewpoint again applies, and transition is deferred to higher Re. For quadratic flow, friction factors exhibit similar behavior -- f increases as relative roughness increases from 0.26 to 0.43, but thereafter it too decreases.

4.3 Results for Other Phase Angles.

Figures 8 a-f show the dependence of friction factor upon phase angle for the six relative roughnesses investigated. Several runs do not extend to Reynolds numbers greater than those at the linear to non-linear transition regime because of constraints upon flow rate due to blower and flow meter limitations. For the two smaller roughnesses, k/D = 0.26 and 0.32, the friction factor-Reynolds number relation in the linear regime was not a function of phase angle, the variance in f at a given Re being less than 2%, irrespective of phase angle. For these low roughnesses the mean flow is still primarily in the x direction, i.e., the macroscopic view prevails, and while the roughness still disturbs the flow near the wall, the phase angle, or in other words, the streamwise location of the roughness, has no significant effect on the pressure loss. This is not the case when the relative roughness is larger. Then much of the flow tends to follow the convoluted roughness surface. Now the phase angle is quite important, and as we saw earlier for the $\phi = 180°$ runs, the friction factor can be reduced due to the micro-channeling effect and can even closely approach the perfectly smooth value of 48/Re which pertains when $\phi = 180°$. This is particularly apparent for k/D = 0.43, Figure 8c, in which f decreases as ϕ increases from 0 to 180°, and the trend becomes more pronounced as k/D increases from 0.51 to 1.26 (Figures 8d, e, and f). For these latter three roughnesses the opposing peaks are nearly in contact when the phase angle is small, so, as expected, small ϕ results in very large friction factors.

Table 2 summarizes the quadratic flow friction factors. We found that when the relative roughness was as small as 0.26, f was independent of ϕ. However, for $k/D \geq 0.32$, f increased as ϕ approached 0°, and this effect is due to narrowing of the flow passage area as the opposing sawtooth peaks approach each other. Note once again, for $\phi = 180°$, that as k/D increased, the flow became smoother and f diminished.

5.0 DISCUSSION

The effect of joint roughness on fluid flow is difficult to deal with because there are so many geometrically different types of roughness. The size, the shape, the density of roughness elements, their relative height compared to the channel width, are all effects that must be taken into consideration. For example, even if the projection from the wall into the flow is the same, providing the same

Table 2.
Friction Factors For Quadratic Flow

Relative Roughness k/D	$\phi = 0°$	$\phi = 60°$	$\phi = 120°$	$\phi = 180°$
0.26	0.4	0.4	0.4	0.4
0.32	2.0	1.9	1.5	1.5
0.43	8.8	6.0	5.0	4.0
0.51	--	3.4	--	2.6
0.64	--	--	--	1.5
1.26	--	--	--	0.5

value of relative roughness, the effect of sharp roughness elements is different than that of smooth sinusoidal variations in the wall surface. A particularly graphic illustration of the importance of roughness geometry was provided by the present results for $\phi = 180°$, that is when the opposing peaks and valleys of the roughness were in phase. It was found that, paradoxically, as the relative roughness increased the friction factor approached that of flow in a perfectly smooth duct. In reality, a microscopic viewpoint of flow in a series of individually smooth ducts was simply becoming more valid. At the opposite end of the spectrum were the results at $\phi = 0°$, where the peaks were in phase. As k/D approached 0.51, i.e., when the peaks of the sawtooth roughness used in the present study would be in contact, the friction factor approached infinity. These two examples should suffice to demonstrate that relative roughness by itself is insufficient to characterize flow in rough joints.

Most joints in nature are "closed," that is, the roughness asperities contact. Thus the the size of the protrusions into the flow channel is of the same order of magnitude as the channel itself, so k/D is of order 0.5 to 1.0. For such large roughness acceleration and deceleration of the flow is caused by the convergent-divergent nature of the flow as it passes through roughness-constricted areas. These repeated acceleration and deceleration sequences cause a departure from a linear pressure loss-flow rate relationship, even if the flow remains laminar. Additional insight into this effect is provided by assuming that the roughness can be approximated as hemispheres. Take the case where the roughness, or sphere diameter, is equal to the equivalent hydraulic diameter, so that, for simplicity, the Reynolds number is the same based upon either diameter. The Oseen solution (Schlichting, 1979) for laminar flow around such a sphere results in the drag coefficient:

$$C = \frac{24}{Re}\left(1 + \frac{3}{16} Re\right)$$

The drag coefficient, C, is the proportionality coefficient between the pressure loss acting on the frontal area of the sphere and the dynamic pressure, $\rho V^2/2$. Where Re is 1 or less the second term, 3 Re/16, is small compared to one. Thus C is inversely proportional to Re, or $C \propto V^{-1}$, so that the pressure loss scales linearly with velocity. However, when Re is 10 or greater, the dynamic pressure loss, which scales with $\rho V^2/2$, is at least as important as the purely viscous, linear pressure loss. Although this analogy is far from perfect because the roughness in the present study cannot be treated as a series of isolated spheres, nevertheless it is clear that

a transition from linear to non-linear flow can be expected in very rough fractures at low Reynolds numbers. The linear to non-linear flow transition can be expected at Reynolds numbers substantially lower than 2000, which usually is taken as the lower value of laminar-to-turbulent transition in a duct. In the present study the transition from linear to non-linear flow occurred at Reynolds numbers as low as 30.

REFERENCES

1. G. M. Lomize, Water Flow in Jointed Rocks (Russian), Gosenergoizdat, 1951.

2. H. Schlichting, Boundary Layer Theory, 7th Ed., McGraw-Hill, New York, pp 116, 1979.

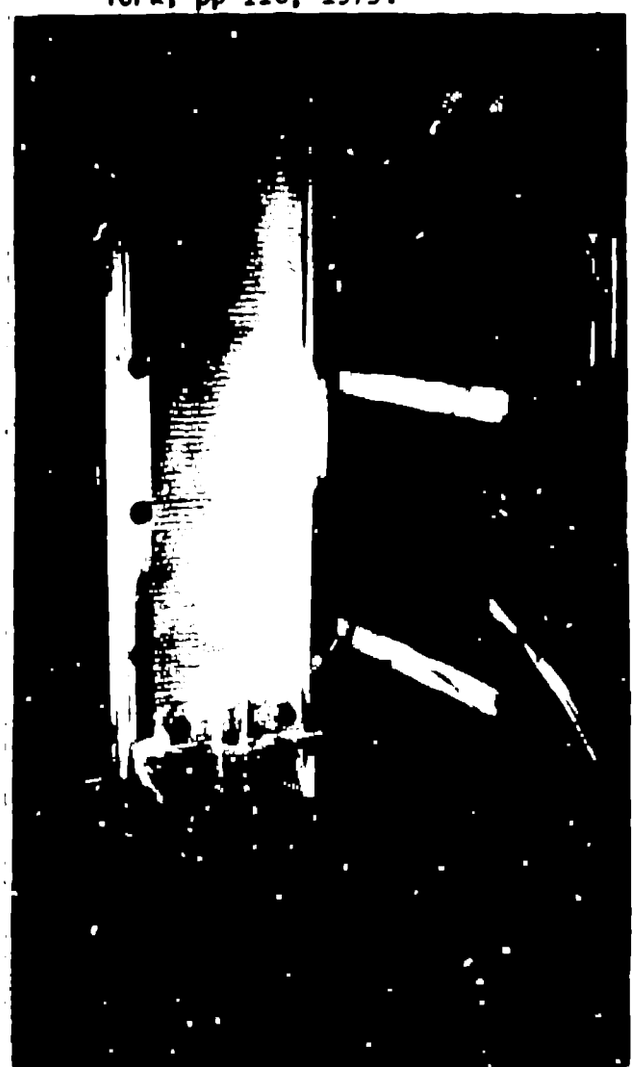

Figure 1.
Photograph of the test apparatus.

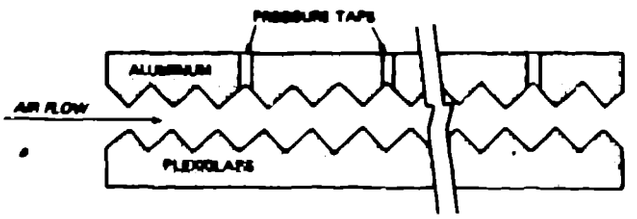

Figure 2.
Test section.

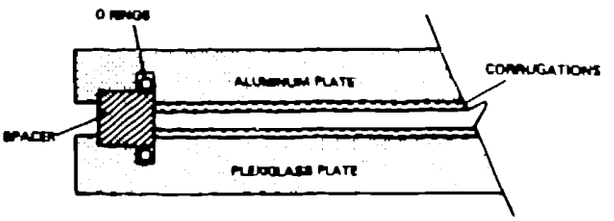

Figure 3.
View of flow test section in flow direction.

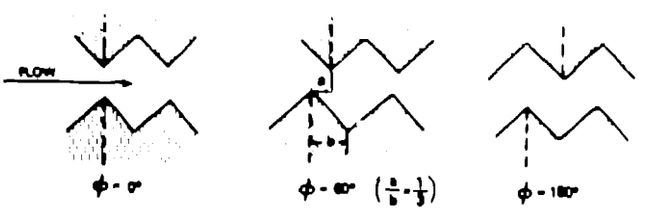

Figure 4.
Phase angles.

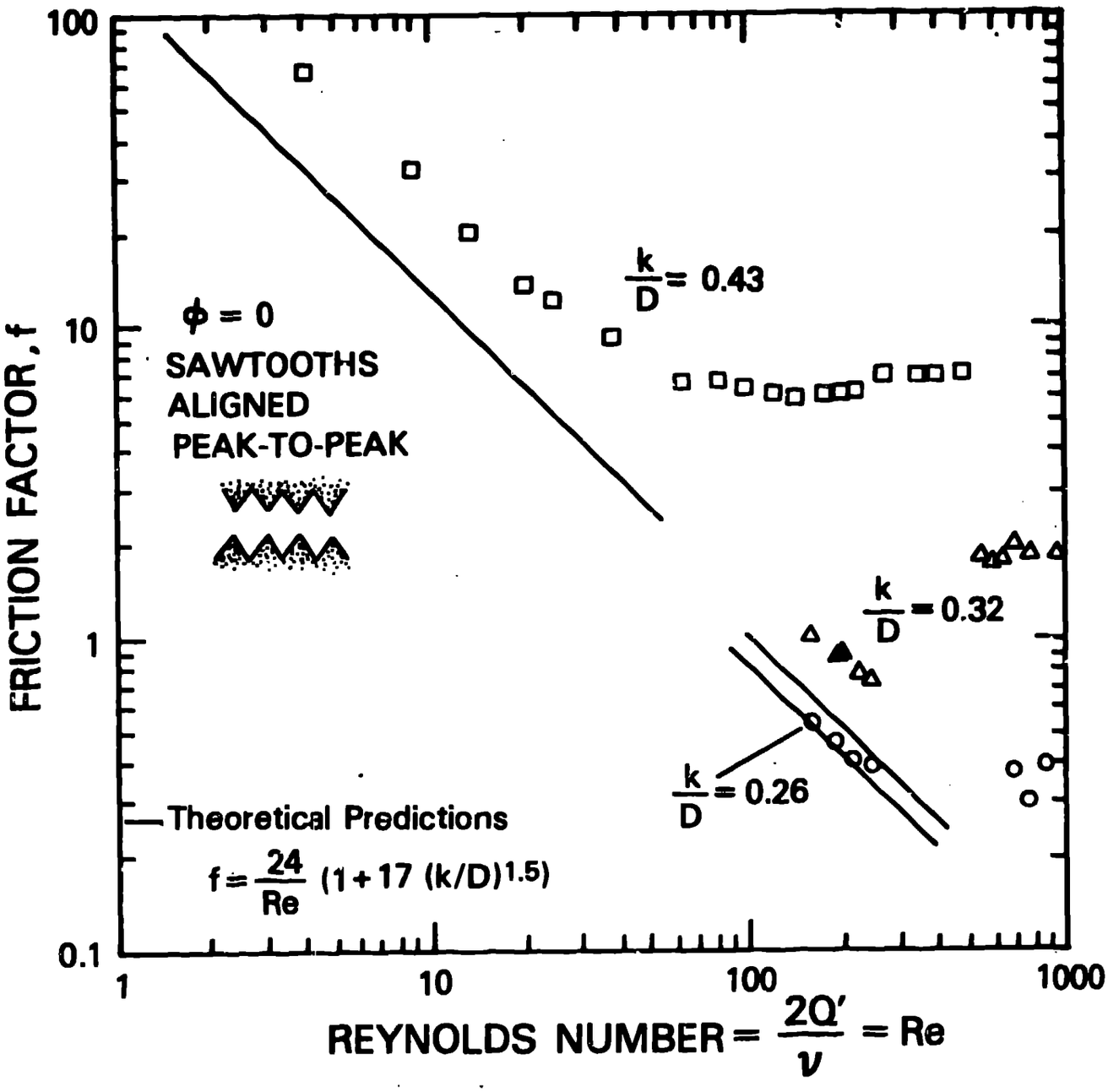

Figure 5.
Data for $\phi = 0$. The equations represent a fit to the data using the general form suggested by Lomize.

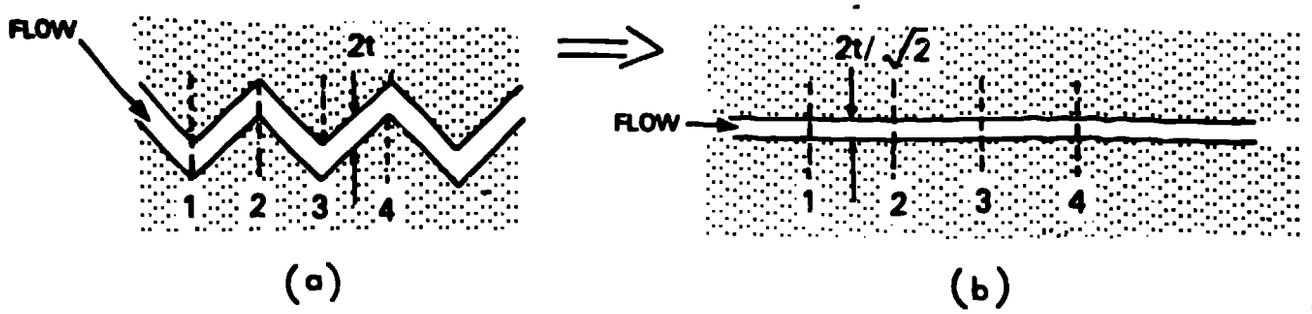

Figure 6.
Small spacing representation. When the flow spacing is small, the flow channel can be represented as a straight, smooth channel.

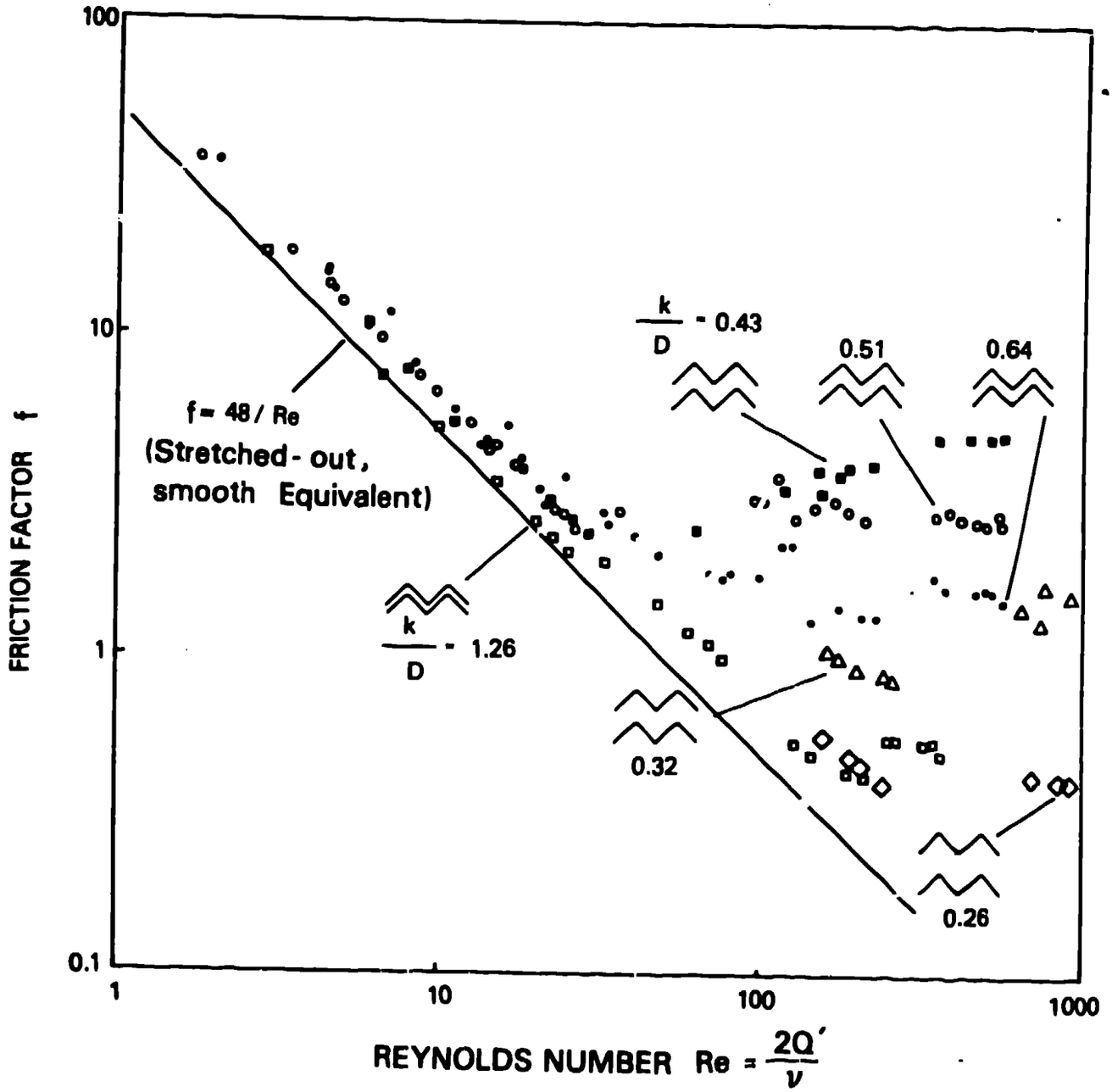

Figure 7.
Friction factor results for cases where peaks and valleys aligned, $\phi = 180°$.

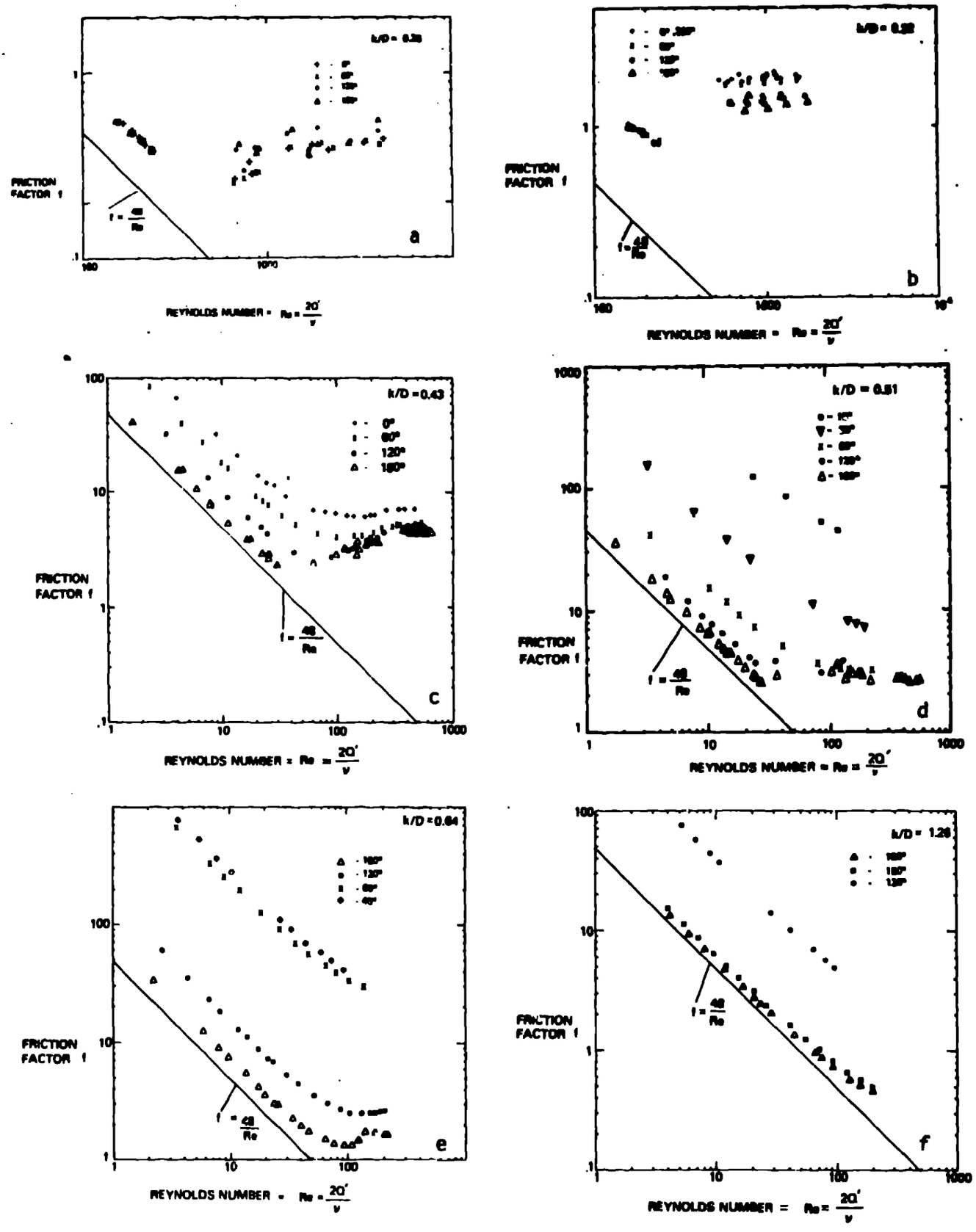

Figures 8 (a-f).
Friction factors for other phase angles.